Influence of interface steps on the buckle delamination of thin films

G. Parry, S. Hamade, J. Durinck, C. Coupeau, Jérôme Colin

Version of Record: https://www.sciencedirect.com/science/article/pii/S0022509619305824
Manuscript_5a44593c778d583c4db71d393cb40aa9

Influence of interface steps on the buckle delamination of thin films

G. Parry

Université de Grenoble-Alpes, CNRS, Grenoble INP, SIMAP, F-38000 Grenoble, France

S. Hamade, J. Durinck, C. Coupeau, J. Colin

Institut P', Université de Poitiers, ENSMA, SP2MI-Téléport 2, 86962 Futuroscope-Chasseneuil cedex, France

Abstract

The mechanics of thin film buckle delamination has been widely studied, with the assumption of perfect (flat) interfaces. This work is reporting a study of the evolution of an initially straight-sided buckle propagating in a thin film lying on a substrate in the presence of a step at the film/substrate interface, resulting from the plastic deformation of the substrate. Assuming the interface toughness depends on the mode mixity, it has been found using finite elements calculations that depending on the step orientation and height, the initially straight propagation of the buckle can be perturbed so that the buckle eventually propagates along the step. The critical parameters (orientation and height) of the step have been then determined, which characterizes the transition from a straight propagation perpendicular to the compression axis to a propagation along the inclined step. A "behavior" diagram has been finally presented for the buckle, where the propagation, either perpendicularly to the step or along it have been displayed versus the step height and orientation.

Keywords: Buckling, Delamination, Layered Material, Finite Elements

1. Introduction

The mechanical properties of thin films on substrates and more generally of multilayered structures have been the topics of intensive research in the fields of materials science, metallurgy and solid mechanics, because of the numerous applications of such structures in several engineering fields such as microelectronics (Freund and Suresh, 2004) or aeronautics for example (Chen et al., 2003). It is now well admitted that during the deposition processes, high residual stress reaching sometimes several gigapascals are generated in the layers (Drory et al., 1988; Girault et al., 2006). When these residual compressive stresses reach critical values, the interfaces can delaminate and the layers buckle (Gille and Rau, 1984; Spiecker et al., 2006). Various buckle morphologies such as straight-sided (Coupeau et al., 1999; Coupeau, 2008), circular (Colin et al., 2009; Kuznetsov et al., 2012), telephone-cord (Moon et al., 2004; Faulhaber et al., 2006) buckles or network-like buckling structures (Ni and Soh, 2014) have been thus observed at the nano- and micro-scales with the help of atomic force and optical microscopes. Likewise, the effect of pressure mismatch between the

upper and lower surfaces of the delaminated films has been studied and the re-deposition and snap-through phenomena have been analyzed versus the pressure and internal stress (Colin et al., 2014). Recently, the plasticity of the films has been considered and the buckle morphologies have been characterized when plastic folding is considered at the circumference or at the top of the buckles (Colin et al., 2007; Durinck et al., 2008; Foucher et al., 2006). The ageing of such buckles has been also investigated and the formation of telephone-cord structures has been explained by the secondary buckling of straight-sided buckles (Thouless et al., 1992; Audoly, 1999; Colin et al., 2000; Audoly et al., 2002; Chai et al., 1981; Parry et al., 2006) as well as the formation of donut- and croissant-like structures from initially circular buckles, considering the coupled effects of plasticity and pressure (Hamade et al., 2015). The propagation of the buckles and the interface delamination have been also widely investigated and the concept of mode mixity (i.e. relative proportion of shear traction component as compared to normal traction component) dependence of the interface toughness has been introduced as a key ingredient for the description of interface cracks at the decohesion fronts of the buckle (Hutchinson and Suo, 1992). In particular, the fact that straight sided buckles indefinitely propagate along their longitudinal axis without lateral expansion has been explained. Recently, finite element simulations have been carried out to explain the propagation of telephone-cord buckles including an adhesion work dependence on the mode mixity (Faou et al., 2012). The pinning of the buckle front in mode II has been thus found to be responsible of the corresponding configurational telephone-cord instability. At the microscopic scale, it has been shown that a variety of interface imperfections such as fracture zone (Cordill et al., 2005; Abdallah et al., 2011), roughness (Evans et al., 1997; Mumm and Evans, 2000) and chemical impurity (Wang and Evans, 1998) can be preferential areas where the interface delamination may start. Likewise, atomic steps at the interfaces (Storåkers and Nilsson, 1993; Foucher et al., 2006) have been identified as topological defects resulting from the plasticity of the multilayered structures where the delamination process can be initiated. Indeed, it has been recently found by means of atomistic simulations that interface steps can play a key role on the interface delamination and lead to interfacial gliding at the edges of buckles providing a physical explanation of the limited growth of the buckle (Ruffini et al., 2013b). Likewise, for Cu-Zr systems, the buckling and post-buckling behaviors have been analyzed versus the film deformation and film thickness (Wu et al., 2019). For titanium nitride films deposited on stainless substrates, the cracking and buckling phenomena have been also investigated for low and strong adhesion energy (Guo et al., 2019).

In the context of the finite element investigations of interface delamination and thin film buckling (Faou et al., 2012; Nilsson, 1995; Jensen and Sheinman, 2002; Gruttmann and Pham, 2007), the study of the complex interactions between crack propagation, buckling and interface imperfections such as atomic steps thus appears as a challenging area of research that could provide a more complete description of the thin film ageing. It is the topic of the present work to investigate, from a numerical point of view through finite element simulations, the influence of an interface step on the propagation of a straight-sided buckle. The Paper is organized as follows. The experimental evidences of buckle propagation in the vicinity of interface steps are first presented for a Ni thin film deposited on a LiF substrate. The modeling technique is then described and the coupled effects of the mixed mode in-

terface toughness and interface steps are discussed on the buckle propagation. Finally, the influence of the step height and step orientation with respect to the compression axis has been analyzed.

2. Buckle observations above a stepped interface

Ni thin films of thickness $h = 150\,\text{nm}$ have been deposited by sputtering physical vapor methods on the (001) surface of LiF single crystals. The coated samples were then plastically deformed up to $\epsilon_p = 2\%$ by uniaxial compression of the substrate along the $[\bar{1}10]$ direction (Fig. 1a). As expected from Schmid factors, the slip system $(0\bar{1}1)[011]$ was activated, leading to slip traces lying along the [100] direction at $\alpha = 45°$ from the compression axis. The slip traces are located in this case at the interface between the film and the substrate (Foucher et al., 2006) and make an emerging angle of $\theta = 45°$ with respect to the (001) plane. The out-of-plane displacements of these steps can be observed on the lower right part of the optical observation presented in Fig. 1b. Straight-sided buckles are also evidenced in Fig. 1b (see the upper part), propagating at 45° from the compression axis. A characteristic profile shown in Fig. 1c demonstrates that the buckles are located just above the steps. In this case, the height H of the three involved slip traces (normalized over the thickness of the film) are equal to $\tilde{H} = 1.3$, 1.3 and 2.0 respectively. This result clearly evidences that the buckles preferentially propagate along the step rather than perpendicularly to the compression axis, as however expected from usual mechanical considerations in the case of a flat surface. One question naturally emerges concerning the possibility for buckles to select their own directions of propagation when the step and the compression axis are not perpendicular. It is the topic of this work to numerically determine the conditions and relevant parameters for such a step-induced deviation to occur.

3. Modeling

The following simulations of the interface delamination, thin film buckling and buckle propagation have been performed with the help of the finite element software ABAQUS using an explicit formulation (Abaqus, 2013). A geometrically non-linear plate lying in the (Oxy) plane is used to model the thin film of thickness h (see Fig. 2a for axes). The plate described in the (Oxy) plane by a square flat domain of length L and width l has been meshed with the help of triangular shell elements. Half of a delaminated disc (hd) of diameter b_{hd} has been introduced as an adhesion-free domain at $x = 0$, in the left part of the film, to initiate the buckling once an internal compressive stress has been applied to the film. The out-of-plane displacement along the (Oz) axis is labeled w, the in-plane ones along (Ox) and (Oy), u and v, respectively. The substrate surface is modeled by a rigid plane such that the plate displacements in the lower half-space are not allowed within this unilateral contact description. The film-substrate interface is described by a cohesive zone model. The film-substrate structure has been submitted to two consecutive loading operations:

- Introduction of the interface step

As shown by Foucher et al. (2006) and Ruffini et al. (2013b), an uniaxial compressive deformation of a coated substrate leads to the emergence of dislocations at the film/substrate interface, which results in the formation of an interface step whose height is of the order of the nanometer. In order to mimic the formation of the interface step, an out-of-plane displacement $w = H$ where H is the step height, has been imposed at the interface region that is located under the right part of the film. This step is thus formed along a slip plane inclined at an angle $\theta = 45°$ with respect to the interface plane which corresponds to the shearing of the substrate along the slip plane (110) (see Fig. 2b). The step direction is inclined at an angle α with respect to the (Oy) axis which is the natural direction for the straight-sided buckle to propagate in case of a flat interface. A displacement field is thus imposed on the right part of the cohesive elements, the left part being fixed to zero (see Fig. 2b) such that:

$$u = -H \sin \alpha, \tag{1}$$

$$v = -H \cos \alpha, \tag{2}$$

$$w = H. \tag{3}$$

At the end of this loading operation, a delaminated part of the film is formed above the step as a strip of width b.

- Application of the residual stress

  During the second step, in order to generate a compressive residual stress in the simulation, a thermal expansion is applied to the plate with components $\epsilon_{yy} = \epsilon_0$ and $\epsilon_{xx} = -\nu_f \epsilon_0$, with $\epsilon_0 > 0$. The expansion is actually restrained by the rigid substrate in the initial unbroken flat state, so that the actual total strain components in the film are zero. The eigenstrain created by the thermal expansion is therefore compensated by exactly opposite elastic strain components, generating a uniaxial compressive stress state:

$$\sigma_{xx} = 0, \tag{4}$$

$$\sigma_{yy} = -E_f \epsilon_0 = -\sigma_0. \tag{5}$$

  The Young's modulus and Poisson ratio of the film are labeled E_f and ν_f, respectively. The following boundary conditions have been considered on both plate edges lying along the (Ox) axis:

$$v = 0, \tag{6}$$

$$\frac{\partial w}{\partial y} = 0. \tag{7}$$

In the following, the non-dimensional parameters $\tilde{H} = H/h$, $\tilde{x} = x/h$, $\tilde{y} = y/h$, $\tilde{w} = w/h, \tilde{b} = b/h, \tilde{b}_{hd} = b_{hd}/h$ and $\tilde{b}_c = b_c/h$ have been introduced, where b_c is the critical width for the buckle to appear on the stepped film/substrate interface whose implicit expression writes (Ruffini et al., 2013a):

$$\epsilon_0^{tr} = \frac{\pi^2}{3}\frac{1}{\tilde{b}_c^2} + \frac{3}{4}\frac{\tilde{H}^2}{\tilde{b}_c^2} - \frac{\tilde{H}}{\tilde{b}_c \tan\theta}, \tag{8}$$

with $\epsilon_0^{tr} > 0$, the critical transversal strain related to ϵ_0 through the relation:

$$\epsilon_{y'y'} = -\epsilon_0^{tr} = -\epsilon_0(\cos^2\alpha - \nu_f \sin^2\alpha), \tag{9}$$

where $\epsilon_{y'y'}$ is the strain applied along the (Oy') direction perpendicular to the step. In order to study the interface delamination, the dependence of the interface toughness with mode mixity has been considered (Hutchinson and Suo, 1992). The dimensionless interface toughness per unit area is then given by (Freund and Suresh, 2004; Ruffini et al., 2013b,a):

$$\tilde{\Gamma}_c(\psi) = \frac{\Gamma_c(\psi)}{G_0}, \tag{10}$$

with G_0, the elastic energy per unit area stored in the film under the uniaxial compression described in Eqs. 4 and 5:

$$G_0 = \frac{h{\sigma_0}^2}{2E_f}. \tag{11}$$

Quadrilateral shell elements are used to mesh the film whose element size is chosen such that the delaminated strip of the film for the minimal value of b obtained after the first loading operation is divided into 20 of those elements. The plate length is $\tilde{L} = L/h = 500$ and its width $\tilde{l} = l/h = 250$.

A mixed-mode cohesive zone model is used to describe the interface rupture (as described in Faou et al. (2012)). Cohesive elements are inserted between the plate elements and the substrate. The traction versus separation law is linear/softening. The traction component normal to the (Oxy) interface plane is denoted T_n, and the shear traction component, T_s (lying in the (Oxy) plane). An effective traction stress T_e can be thus defined for the mixed mode as $T_e = \sqrt{T_n^2 + T_s^2}$. The interface behavior is linear and reversible ($\overrightarrow{T} = K\overrightarrow{\delta}$) until a peak traction is reach. The peak values for the traction components is defined by a quadratic criterion:

$$\left(\frac{T_n}{T_n^0}\right)^2 + \left(\frac{T_s}{T_s^0}\right)^2 = 1, \tag{12}$$

At this threshold marking damage initiation, the values $T_n^{'}$ and $T_s^{'}$ are taken by T_n and T_s respectively, leading to $T_e^{'} = \sqrt{(T_n^{'})^2 + (T_s^{'})^2}$. Once this criterion is achieved, the mode mixity is evaluated depending on the mixity of the loading described by the angle ψ:

$$\tan(\psi) = \frac{T_s^{'}}{T_n^{'}}, \tag{13}$$

The normal T_n, shear T_s and effective T_e tractions have been plotted in Fig. 3 as a function of the normal δ_n, shear δ_s and effective $\delta_e = \sqrt{\delta_n^2 + \delta_s^2}$ separations respectively, for pure normal (mode I), pure shear (mode II) and mixed mode loadings. For the I and II pure loading modes, the tractions T_n and T_s linearly increase when the relative normal δ_n and shear δ_s displacements increase, with K the loading stiffness defined as $K = T_n^{'}/\delta_n^{'} = T_s^{'}/\delta_s^{'}$, where $T_n^{'}$ and $T_s^{'}$ are the maximum values of T_n and T_s obtained for $\delta_n^{'}$ and $\delta_s^{'}$, respectively. It is also underlined that T_n and T_s linearly decrease for $\delta_n > \delta_n^{'}$ and $\delta_s > \delta_s^{'}$ and finally vanish at δ_n^f and δ_s^f, respectively. This second decreasing regime describes the damage of the cohesive elements that have been modeled introducing the interface toughness per unit area:

$$\Gamma_c(0) = G_I^c = \frac{1}{2} T_n^{'} \delta_n^f, \tag{14}$$

for pure mode I and:

$$\Gamma_c(\pi/2) = G_{II}^c = \frac{1}{2} T_s^{'} \delta_s^f, \tag{15}$$

for pure mode II. For the mixed mode loading, the first reversible regime is characterized by an effective traction T_e linearly increasing with its relative displacement δ_e, with $\delta_e < \delta_e^{'}$. using the expression of $\Gamma_c(\psi)$ given by Hutchinson and Suo (1992):

$$\Gamma_c(\psi) = G_I^c[1 + \tan^2(\eta\psi)], \tag{16}$$

where η is a parameter determined by the condition $\Gamma_c(\pi/2) = G_{II}^c$, corresponding to the effective adhesion energy in pure mode II. The second regime is then characterized by the irreversible decrease of T_e as δ_e increases until it vanishes when δ_e reaches its final value $\delta_e^f = 2\Gamma_c(\psi)/T_e^{'}$. In the framework of this model, the simulations have been performed using the following parameters for the film. The elastic modulus $E_f = 205\,\mathrm{GPa}$, the Poisson ratio $\nu_f = 0.30$ are considered for an elastic plate of thickness $h = 20\,\mathrm{nm}$. A value $\epsilon_0 = 0.59\%$ is taken for the eigenstrain parameter in the plate leading to the resulting uniaxial compressive stress $\sigma_0 = 1200\,\mathrm{MPa}$. The non-dimensional adhesion-free half-disk width is $\tilde{b}_{hd} = 50$. The ratios between the adhesion energy and the elastic energy G_0 have been taken to be $G_I^c/G_0 = 0.546$ and $G_{II}^c/G_0 = 88.7$ (corresponding to a value $\eta = 0.95$) for the modes I and II, respectively. The maximum cohesive tractions are then $T_n^0 = 0.02\sigma_0$ and $T_s^0 = 0.24\sigma_0$ and the stiffness is $K = 6.6 \times 10^2 (T_n^0)^2/G_0$.

4. Results and Discussion

4.1. Buckle propagation on a stepped interface

The formation (at $\epsilon_0 = 0$) of the step of height $\tilde{H}$ has generated a delaminated strip of the film of width b. The values of $\tilde{b}$ obtained for different values of $\tilde{H}$ ranging from 0.05 to 0.30 have been first extracted and plotted in Fig. 4 versus $\tilde{H}$, together with the critical buckling width $\tilde{b}_c$ defined in Eq. (8). It is observed in this Fig. 4 that although $\tilde{b}$ linearly

increases with $\tilde{H}$, it is always below the critical buckling width $\tilde{b}_c$ calculated for $\epsilon_0 = 0$. This explains why the delaminated strip of the film does not spontaneously buckle once the step is formed at $\epsilon_0 = 0$. When the system is under strain, *i.e.* for $\epsilon_0 = 0.59\%$, the critical value $\tilde{b}_c$ depends on α angle. For the different considered values of α (10°, 15°, 20°, 25°), $\tilde{b}$ is still below $\tilde{b}_c$ despite its α-dependence. The film is thus not assumed to buckle above the step when the strain ϵ_0 is applied to it. On the other hand, the initially delaminated half-disk has been sized such that it is allowed to buckle, its diameter $\tilde{b}_{hd} = 50$ being chosen larger than the critical value.

In order to illustrate the effect of the interface steps on the propagation of a buckle from the half-disk of the film already delaminated and buckled, two snapshots at two different times t_1 and t_2 have been first presented in Figs. 5a and b, for a planar ($\tilde{H} = 0$) and stepped ($\tilde{H} = 0.30$) interface, with $t_2 > t_1$. Applying the loading procedure described in the previous section, it is observed in Fig. 5a that, in case of a planar interface, the straight-sided buckle propagates along the (Ox) axis perpendicular to the compression axis (Oy), leading thus to the formation of the classical Euler column (Hutchinson and Suo, 1992). When an interface step with an tilt angle $\alpha = 10°$ with respect to (Ox) axis is considered, it is found in Fig. 5b that the buckle is progressively deviated by the step and at time t_2, the buckle is observed to be aligned with the step. Beyond these two extreme cases, the problem of the determination of the relevant parameters controlling the buckle deviation such as the deviation angle or step height for example can be raised. This point is addressed in the next subsection.

4.2. Influence of the interface step height and tilt angle on the buckle propagation

In order to characterize the deviation of the buckle in the vicinity of the step, the following procedure has been used. For each buckle, the maximum deflection of the film has been plotted in Figs. 6 in the (Oxy) plane, the tilt angle α being fixed to 10° in a first time. In Fig. 6a, it is observed that starting from the straight-sided buckle propagating along the (Ox) axis in case of a plane interface (black line) when $\tilde{H} = 0$, the buckle propagation is perturbed by the step as its height increases until 0.3. At this point, it has to be underlined that the ultimate buckle deviations observed at the end of the simulations (in the region $\tilde{x} = 500$) have been checked (but not shown) to be a numerical artifact due to the size of the simulation box. To determine for this particular angle $\alpha = 10°$, the critical height beyond which the buckle is definitely attracted by the step, the size of the simulation box has been increased ($\times 3$) and adjusted to avoid the boundary effect in Fig. 6b, where it can be deduced that the changing in the buckle direction occurs for $0.15 < \tilde{H} < 0.2$. Indeed, for $\tilde{H} = 0.15$, the buckle overcomes the step attraction and recovers its (Ox) direction of propagation, while for $\tilde{H} = 0.2$ the buckles finally follows the step direction. In the following, this procedure consisting in enlarging the simulation box has been applied each time it is required for the determination of $\tilde{H}_c$ to avoid the boundary artifact.

The next step of the present work has been to determine the variation of this critical height $\tilde{H}_c$ as a function of the tilt angle α of the step with respect to the compression axis. To do so, the maximum of the buckle deflection has been plotted versus $\tilde{x}$ and $\tilde{y}$ for $\tilde{H} \in [0, 0.30]$ and $\alpha = 15°, 20°$ and 25° in Figs. 7. It is observed that as the tilt angle of the step with respect to the compression axis increases, the propensity of the step to capture the

buckle decreases. For $\alpha = 25°$ in Fig. 7c, although locally modified, the buckle trajectory always expands beyond the step, whatever $\tilde{H}$.

In order to give a physical explanation of this phenomenon identified as buckle deviation, the dimensionless elastic energy density U_{el}/U_0 stored in the stepped film has been first displayed in Figs 8a and 8b, for two values of the step height, *i.e.* $\tilde{H}_1 = 0.15$ and $\tilde{H}_2 = 0.25$, with U_0 the elastic energy stored in the planar film under strain. It is observed that, in both cases, this elastic energy reaches largest values on the step, with maximum values equal to $U_{\text{el}}^{\max 1}/U_0 = 6.3$ and $U_{\text{el}}^{\max 2}/U_0 = 9.1$ for the step heights $\tilde{H}_1$ and $\tilde{H}_2$, respectively. Hence, as soon as the buckle delamination front reaches the step, it tends to deviate towards the step direction in order to increase the strain energy released per unit of delaminated area (i.e. to increase the energy release rate G). In the meantime, propagation towards the vertical direction is optimal in the context of a pure horizontal uniaxial compression. The rotation angle of the buckle therefore sets as a compromise between the additional energy release provided by the step and the high driving force provided by the uniaxial compression. Since a higher value of $\tilde{H}$ offers a higher density of strain energy to be released along the step, it is to be expected that (for a given step tilt angle), the rotation rate of the step per unit length of front propagation will increase with $\tilde{H}$. This is what is observed, for example in Fig. 7.

It is sometimes observed that the buckle tends to start aligning with the step in the first stages of the interaction, then leaves the step to recover a vertical trajectory. In order to explain this, the dependence of the interface toughness with respect to the mode mixity of the loading has to be considered. Everywhere at the crack front, the maximum work of separation that can be spent per unit area corresponds to the whole elastic energy stored in this unit area. This gives a maximum value of the mode mixity angle $\psi_{\max}$ above which the buckle can not propagate (since Γ_c is a monotonically increasing function of ψ). This hence provides a local delamination arrest criterion in terms of ψ:

$$G_{\text{el}}^{\max} = \Gamma_c(\psi_{\max}), \tag{17}$$

where Γ_c is defined in Eq. 16 and $G_{\text{el}}^{\max} = U_{\text{el}}^{\max}/S$, with S the surface of the elements. The evolution of Γ_c/G_{Ic} versus ψ has been then plotted in Fig. 9a for $\eta = 0.95$ and also for $\eta = 0.7$, this last value being discussed later. From this variation in the case where $\eta = 0.95$, three maximum values of the mode mixity angle, $\psi_0 = 40°$, $\psi_{\max}^1 = 76°$ and $\psi_{\max}^2 = 80°$, have been determined for $G_0/G_{Ic} = 1.83$, $G_{\text{el}}^{\max 1}/G_{Ic} = 11.53$ and $G_{\text{el}}^{\max 2}/G_{Ic} = 16.65$, in the case of the planar film and the stepped one with step height $\tilde{H}_1$ and $\tilde{H}_2$, respectively. In Figs 9b and 9c, ψ has been represented on the surface of the film for $\eta = 0.95$ in cases of $\tilde{H}_1$ and $\tilde{H}_2$. In both cases, it is found that the propagation of the right-hand side of the buckle stops once the mode mixity angle has reached the maximum value of 40° already defined. On the other side, at the step location, it appears that for $\tilde{H}_1$, the maximum value of $\psi_{\max}^1$ has been reached, resulting in a propagation front pining somewhat similar to what is observed in Faou et al. (2012), such that the buckle can not propagate along the step anymore and thus deviates (Fig. 9b). Conversely, for $\tilde{H}_2$, the maximum value $\psi_{\max}^2$ of the angle is never reached and the buckle propagates along the step (Fig. 9c). In addition to this analysis,

it is underlined that when η decreases, the toughness of the interface is less sensitive to ψ variations and the interface is considered as more brittle. This point is illustrated for $\eta = 0.7$. Indeed, it is deduced from Fig. 9a (green curve) that no maximum value of ψ can be obtained in the range $[0°, 90°]$ for $\tilde{H}_1$ and $\tilde{H}_2$ when $\eta = 0.7$. As a consequence, the delamination arrest criterion defined in Eq. 17 is never satisfied and the buckle can propagate along the step as shown in Fig. 9d for $\tilde{H}_1 = 0.15$.

In order to characterize the effect of the step on the behavior of the buckle, the critical step height $\tilde{H}_c$ has been determined from Figs. 6 and 7 and has been used to build a propagation diagram for the step in Fig. 10, where the two different behaviors, *i.e.* the propagation beyond or the propagation in the neighborhood of the step have been displayed in the $(\alpha, \tilde{H})$ plane. It is confirmed on this diagram that the "buckle capture" by the step is less and less favorable as the tilt angle of the step increases with respect to the compression axis and the step height decreases.

Finally, it has to be emphasized that, once captured by a step, particular configurations may allow for the buckles to escape from it. It is the case when two buckles propagate towards each other. As an example, the buckle propagation along a step of height $\tilde{H} = 0.3$ and tilt angle $\alpha = 10°$ has been studied in Fig. 11 where two buckles are observed to propagate from the two opposite sides of the simulation box towards its center. It is found in this case that when the two propagating buckles are sufficiently close to each other, they can deviate from their initially straight trajectory due to the repulsive interaction of the two stress fields generated ahead of the propagating fronts. Once the buckles are deviated, they are suspected to propagate perpendicularly to the compression axis, each one lying in a different planar regions of the film.

5. Conclusions

The coupled effects of interface plasticity and mixed mode dependence of the interface toughness has been investigated by means of finite element simulations of the propagation of a buckle appearing in a thin film deposited on a substrate submitted to compressive strain. It has been found from a numerical point of view that the introduction of an interface step can strongly modify the direction of the buckle propagation. Indeed, provided the tilt angle of the step with respect to the compression axis is sufficiently small, the buckle has been found to be captured by the step when its height exceeds a critical value. Based on an analysis of the elastic energy density stored in the vicinty of the step and on the determination of the mode mixity angle, an explanation to the buckle deviation has been proposed through the possibility or not for the mode mixity angle to reach its maximum value when the buckle propagates onto the step. A propagation diagram has been finally displayed versus the height of the step and its tilt angle with respect to the compression axis. The regions characterizing the buckle propagation along the step and far away from it have been thus identified. The possibility that the buckle may escape from the step and propagate towards the planar regions of the film has been finally discussed.

This study shows, for the first time at our knowledge, how buckles can strongly interact with surface heterogeneities during their propagation, and indicate routes for thin films

patterning assisted by controlled heterogeneities through substrate patterning.

For Ni thin films deposited on LiF substrates, the possibility of local deviation of the buckles should be now experimentally investigated. Likewise, numerical simulations coupled with a theoretical analysis of the buckle propagation should be also performed to characterize the mechanical behavior of this particular Ni/LiF system.

6. Acknowledgments

Computations have been performed on the supercomputer facilities of the Mésocentre de calcul Poitou-Charentes.

References

Abaqus, 2013. Manuals Collection. Dassault Systems, Simulia Corp. Providence, RI, USA.

Abdallah, A., Bouten, P., den Toonder, J., de With, G., 2011. Buckle initiation and delamination of patterned ITO layers on a polymer substrate. Surf. Coat. Tech. 205, 3103–3111. doi:10.1016/j.surfcoat.2010.11.025.

Audoly, B., 1999. Stability of straight delamination blisters. Phys. Rev. Lett. 83, 4124. doi:10.1103/PhysRevLett.83.4124.

Audoly, B., Roman, B., Pocheau, A., 2002. Secondary buckling patterns of a thin plate under in-plane compression. Eur. Phys. J. B 27, 7–10. doi:10.1140/epjb/e20020124.

Chai, H., Babcock, C.D., Knauss, W.G., 1981. One dimensional modelling of failure in laminated plates by delamination buckling. Int. J. Solids Struct. 17, 1069–1083. doi:10.1016/0020-7683(81)90014-7.

Chen, X., Hutchinson, J., He, M., Evans, A., 2003. On the propagation and coalescence of delamination cracks in compressed coatings: with application to thermal barrier systems. Acta Mater. 51, 2017–2030. doi:10.1016/S1359-6454(02)00620-1.

Colin, J., Cleymand, F., Coupeau, C., Grilhé, J., 2000. Worm-like delamination patterns of thin stainless steel films on polycarbonate substrates. Philos. Mag. A 80, 2559–2565. doi:10.1080/01418610008216492.

Colin, J., Coupeau, C., Durinck, J., Cimetière, A., Grilhé, J., 2014. Redeposition of a straight-sided buckle under pressure. Phys. Rev. E 89, 032410–032410. doi:10.1103/PhysRevE.89.032410.

Colin, J., Coupeau, C., Durinck, J., Grilhé, J., 2009. Buckling patterns of gold thin films on silicon substrates: Formation of superimposed blisters. Europhys. Lett. 86, 540021–540025. doi:10.1209/0295-5075/86/54002.

Colin, J., Coupeau, C., Grilhé, J., 2007. Plastic Folding of Buckling Structures. Phys. Rev. Lett. 99, 46101–46101. doi:10.1103/PhysRevLett.99.046101.

Cordill, M., Moody, N., Bahr, D., 2005. The effects of plasticity on adhesion of hard films on ductile interlayers. Acta Mater. 53, 2555–2562. doi:10.1016/j.actamat.2005.02.013.

Coupeau, C., 2008. From thin film and coating buckling structures to mechanical properties. Mater. Sci. Eng. A-Struct. 483-484, 617–619. doi:10.1016/j.msea.2006.09.181.

Coupeau, C., Naud, J.F., Cleymand, F., Goudeau, P., Grilhé, J., 1999. Atomic force microscopy of in situ deformed nickel thin films. Thin Solid Films 353, 194–200. doi:10.1016/S0040-6090(99)00369-7.

Drory, M., Thouless, M., Evans, A., 1988. On the decohesion of residually stressed thin films. Acta Metall. 36, 2019–2028. doi:10.1016/0001-6160(88)90303-3.

Durinck, J., Coupeau, C., Colin, J., Grilhé, J., 2008. Molecular dynamics simulations of buckling-induced plasticity. Appl. Phys. Lett. 93, 221904–221904. doi:10.1063/1.3033552.

Evans, A., He, M., Hutchinson, J., 1997. Effect of interface undulations on the thermal fatigue of thin films and scales on metal substrates. Acta Mater. 45, 3543–3554. doi:10.1016/S1359-6454(97)00062-1.

Faou, J.Y., Parry, G., Grachev, S., Barthel, E., 2012. How does adhesion induce the formation of telephone cord buckles? Phys. Rev. Lett. 108, 116102. doi:10.1103/PhysRevLett.108.116102.

Faulhaber, S., Mercer, C., Moon, M., Hutchinson, J., Evans, A., 2006. Buckling delamination in compressed multilayers on curved substrates with accompanying ridge cracks. J. Mech. Phys. Solids 54, 1004–1028. doi:10.1016/j.jmps.2005.11.005.

Foucher, F., Coupeau, C., Colin, J., Cimetière, A., Grilhé, J., 2006. How Does Crystalline Substrate Plasticity Modify Thin Film Buckling? Phys. Rev. Lett. 97, 96101–96101. doi:10.1103/PhysRevLett.97.096101.

Freund, L.B., Suresh, S., 2004. Thin Film Materials: Stress, Defect Formation and Surface Evolution. Cambridge University Press, Cambridge. doi:10.1017/CBO9780511754715.

Gille, G., Rau, B., 1984. Buckling instability and adhesion of carbon layers. Thin Solid Films 120, 109–121. doi:10.1016/0040-6090(84)90365-1.

Girault, B., Villain, P., Le Bourhis, E., Goudeau, P., Renault, P.O., 2006. X-ray diffraction analysis of the structure and residual stresses of W/Cu multilayers. Surf. Coat. Tech. 201, 4372–4376. doi:10.1016/j.surfcoat.2006.08.034.

Gruttmann, F., Pham, V.D., 2007. A finite element model for the analysis of buckling driven delaminations of thin films on rigid substrates. Comp. Mech. 41, 361–370. doi:10.1007/s00466-007-0191-9.

Guo, T., Pang, X., He, J., Zhang, Z., Qiao, L., 2019. Substrate slip steps promote cracking and buckling of thin brittle film. Scripta Mater. 163, 82–85. doi:10.1016/j.scriptamat.2018.12.037.

Hamade, S., Durinck, J., Parry, G., Coupeau, C., Cimetière, A., Grilhé, J., Colin, J., 2015. Effect of plasticity and atmospheric pressure on the formation of donut- and croissantlike buckles. Phys. Rev. E 91, 012410–012410. doi:10.1103/PhysRevE.91.012410.

Hutchinson, J.W., Suo, Z., 1992. Mixed mode cracking in layered materials. Adv. Appl. Mech. 29, 63–191. doi:10.1016/S0065-2156(08)70164-9.

Jensen, H., Sheinman, I., 2002. Numerical analysis of buckling-driven delamination. Int. J. Solids Struct. 39, 3373–3386. doi:10.1016/S0020-7683(02)00158-0.

Kuznetsov, A.S., Gleeson, M.A., Bijkerk, F., 2012. Hydrogen-induced blistering mechanisms in thin film coatings. J. Phys.-Condens. Mat. 24, 052203. doi:10.1088/0953-8984/24/5/052203.

Moon, M.W., Lee, K.R., Oh, K., Hutchinson, J., 2004. Buckle delamination on patterned substrates. Acta Mater. 52, 3151–3159. doi:10.1016/j.actamat.2004.03.014.

Mumm, D., Evans, A., 2000. On the role of imperfections in the failure of a thermal barrier coating made by electron beam deposition. Acta Mater. 48, 1815–1827. doi:10.1016/S1359-6454(99)00473-5.

Ni, Y., Soh, A., 2014. On the growth of buckle-delamination pattern in compressed anisotropic thin films. Acta Mater. 69, 37–46. doi:10.1016/j.actamat.2014.01.041.

Nilsson, K., 1995. A finite element analysis of configurational stability and finite growth of buckling driven delamination. J. Mech. Phys. Solids 43, 1983–2021. doi:10.1016/0022-5096(95)00052-K.

Parry, G., Cimetière, A., Coupeau, C., Colin, J., Grilhé, J., 2006. Stability diagram of unilateral buckling patterns of strip-delaminated films. Phys. Rev. E 74, 66601–66601. doi:10.1103/PhysRevE.74.066601.

Ruffini, A., Durinck, J., Colin, J., Coupeau, C., Grilhé, J., 2013a. Buckling-induced dislocation emission in thin films on substrates. Int. J. Solids Struct. 50, 3717–3722. doi:10.1016/j.ijsolstr.2013.07.015.

Ruffini, A., Durinck, J., Colin, J., Coupeau, C., Grilhé, J., 2013b. Interface step-induced thin-film delamination and buckling. Acta Mater. 61, 4429–4438. doi:10.1016/j.actamat.2013.04.012.

Spiecker, E., Schmid, A.K., Minor, A.M., Dahmen, U., Hollensteiner, S., Jäger, W., 2006. Self-Assembled Nanofold Network Formation on Layered Crystal Surfaces during Metal Intercalation. Phys. Rev. Lett. 96, 086401. doi:10.1103/PhysRevLett.96.086401.

Storåkers, B., Nilsson, K.F., 1993. Imperfection sensitivity at delamination buckling and growth. Int. J. Solids Struct. 30, 1057–1074. doi:10.1016/0020-7683(93)90003-P.

Thouless, M., Hutchinson, J., Liniger, E., 1992. Plane-strain, buckling-driven delamination of thin films: Model experiments and mode-II fracture. Acta Metall. Mater. 40, 2639–2649. doi:10.1016/0956-7151(92)90333-A.

Wang, J.S., Evans, A., 1998. Measurement and analysis of buckling and buckle propagation in compressed oxide layers on superalloy substrates. Acta Mater. 46, 4993–5005. doi:10.1016/S1359-6454(98)00172-4.

Wu, K., Wang, Y., Yuan, H., Zhang, J., Liu, G., Sun, J., 2019. Unique buckling and post-buckling behavior of Cu–Zr amorphous films on compliant substrates. Mater. Lett. 237, 118–121.

doi:10.1016/j.matlet.2018.11.095.

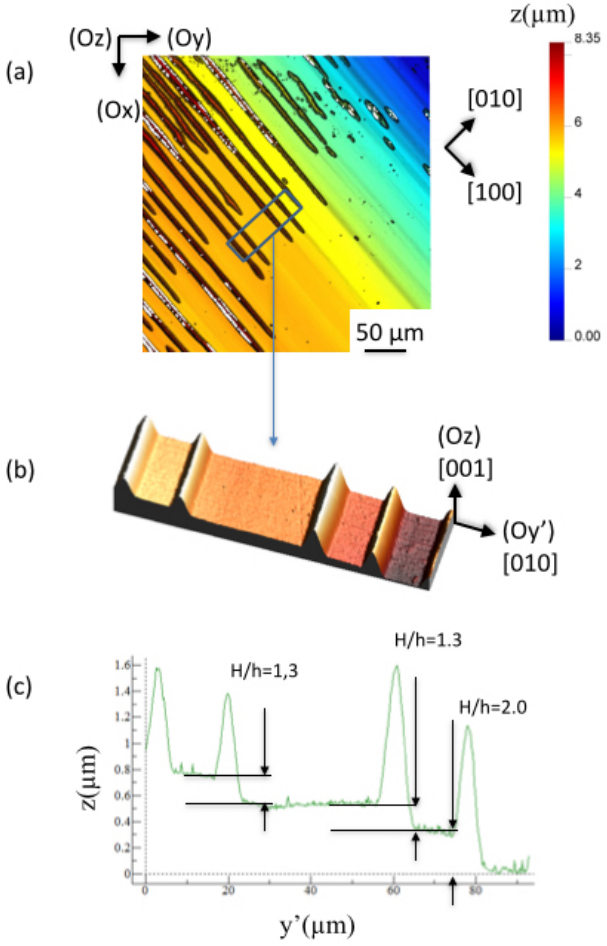

Figure 1: Optical observations of the surface of a Ni thin film deposited on a plastically deformed LiF substrate. (a) General view at the micrometric scale of the buckled surface. (b) AFM observations of the buckles formed above the interface steps. (c) Profile of the thin film surface for the particular area presented in (b).

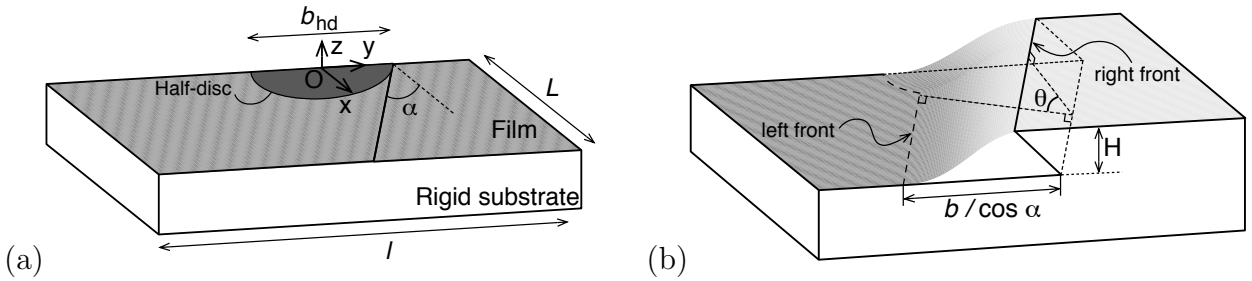

Figure 2: Schematic representation of the thin film on its substrate. (a) The film is initially delaminated on a half-disc of diameter b_{hd}. (b) After the formation of the interface step, a film strip of width b is delaminated along the step.

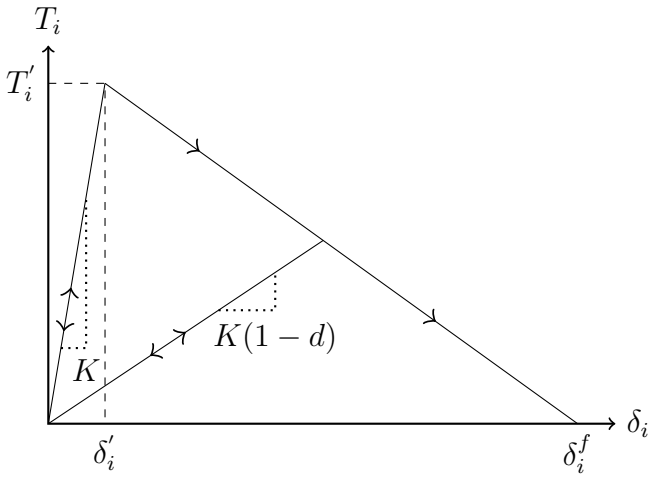

Figure 3: Schematic representation of the material law used for the interface delamination where the traction T_i has been plotted versus the separation δ_i. The I, II and mixed modes are referenced by the indices $i = n, s$ and e respectively.

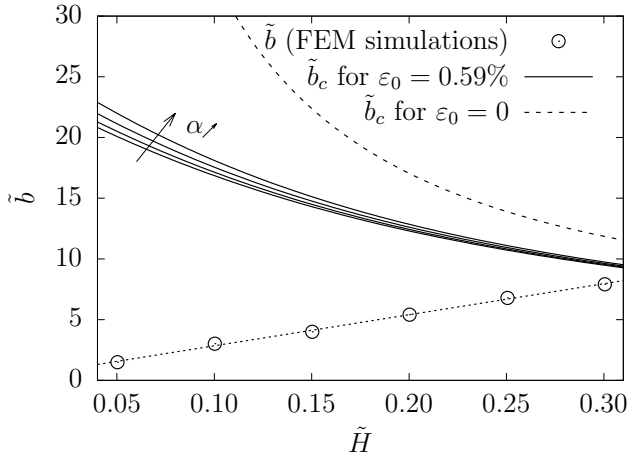

Figure 4: Variation of the width of the delaminated film strip $\tilde{b}$ versus $\tilde{H}$ after the formation of the step. The variations of the critical width $\tilde{b}_c$ versus $\tilde{H}$ have been added for $\epsilon_0 = 0$ and for $\epsilon_0 = 0.59\%$ (see Eq. 8). For $\epsilon_0 = 0.59\%$, different values of the step tilt angle have been considered: $\alpha = 10°, 15°, 20°, 25°$.

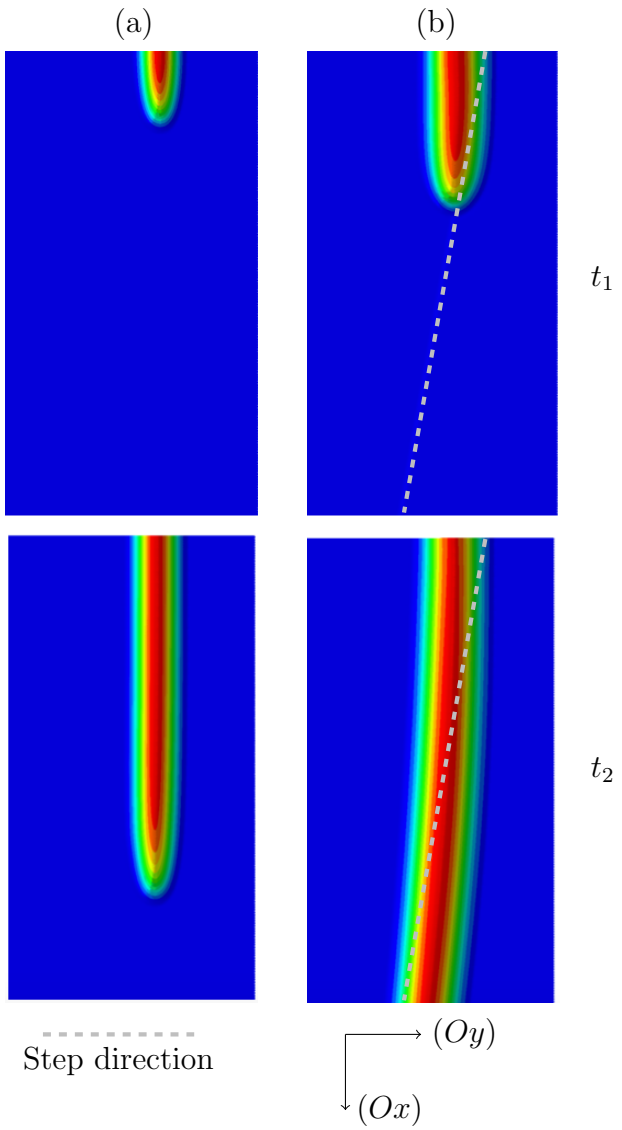

Figure 5: Snapshots of the surface of the film at two different dimensionless time t_1 and t_2 with $t_2 > t_1$. (a) Straight propagation of the buckle in a planar film, along the (Ox) axis, when a uniaxial compressive strain is applied in the (Oy) direction. (b) Inclined propagation of the buckle in the vicinity of a step for $\alpha = 10°$.

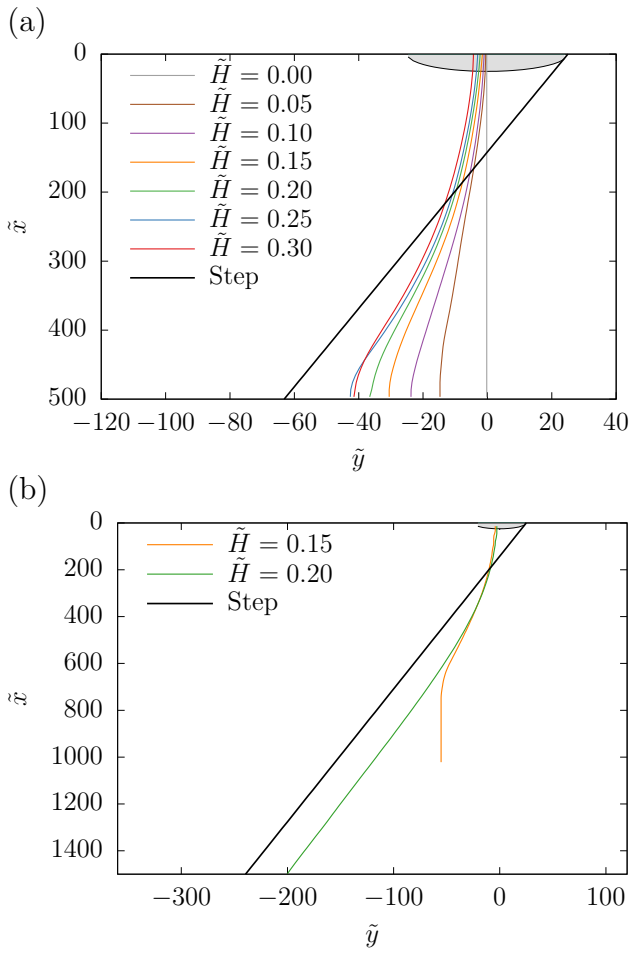

Figure 6: Position in the $(\tilde{x}, \tilde{y})$ plane of the maximum of the buckle deflection for different values of the step height $\tilde{H}$, with $\alpha = 10°$. (a) Buckle positions for increasing values of $\tilde{H}$. (b) For $\tilde{H} = 0.15$, the buckle leaves the step region, for $\tilde{H} = 0.2$, the buckle follows the step.

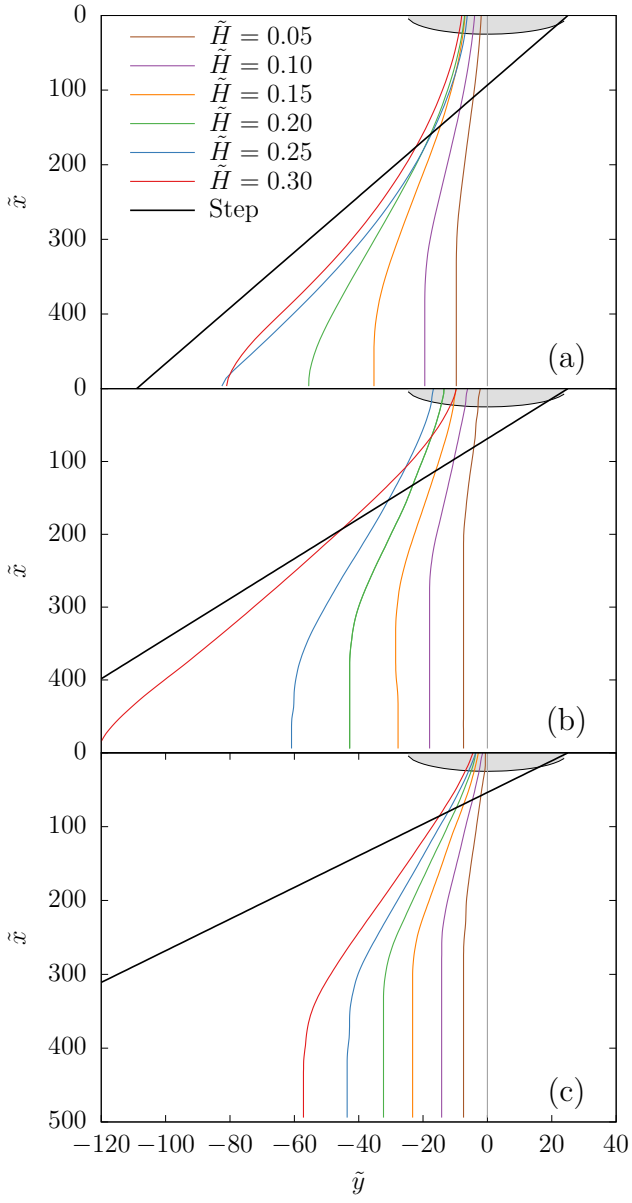

Figure 7: Position in the $(\tilde{x}, \tilde{y})$ plane of the maximum deflection of the buckle for different heights of the step. (a) $\alpha = 15°$. (b) $\alpha = 20°$. (c) $\alpha = 25°$.

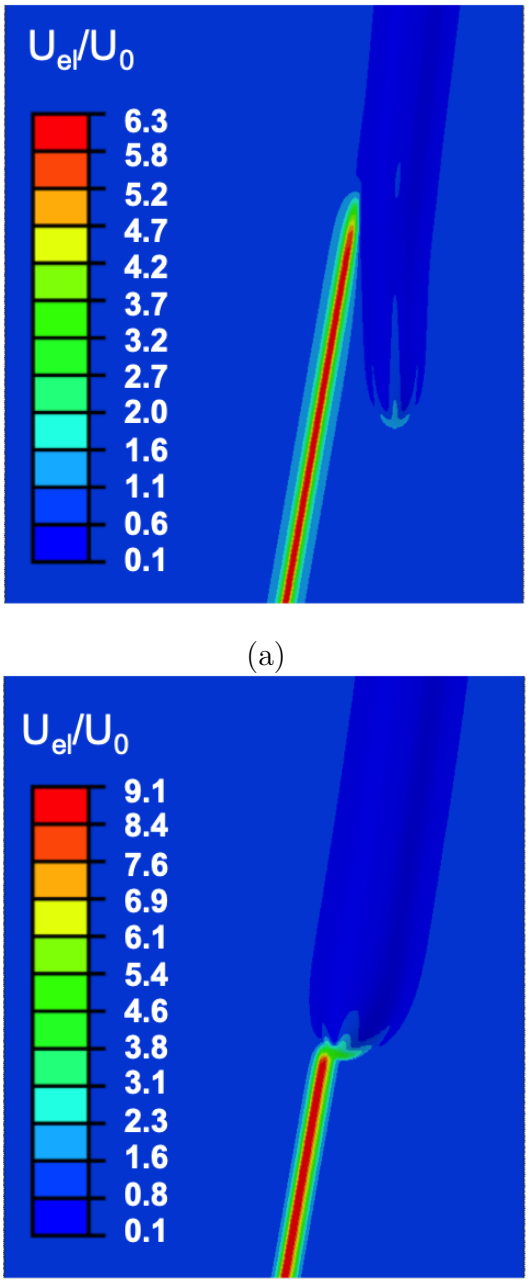

(a)

(b)

Figure 8: Strain energy distribution inside the film during the buckle propagation, normalized with respect to the remote unperturbed value, for two values of the step height and $\alpha = 10°$. Dark blue indicates the lowest energy areas, red the highest. (a) $\tilde{H} = 0.15$. (b) $\tilde{H} = 0.25$.

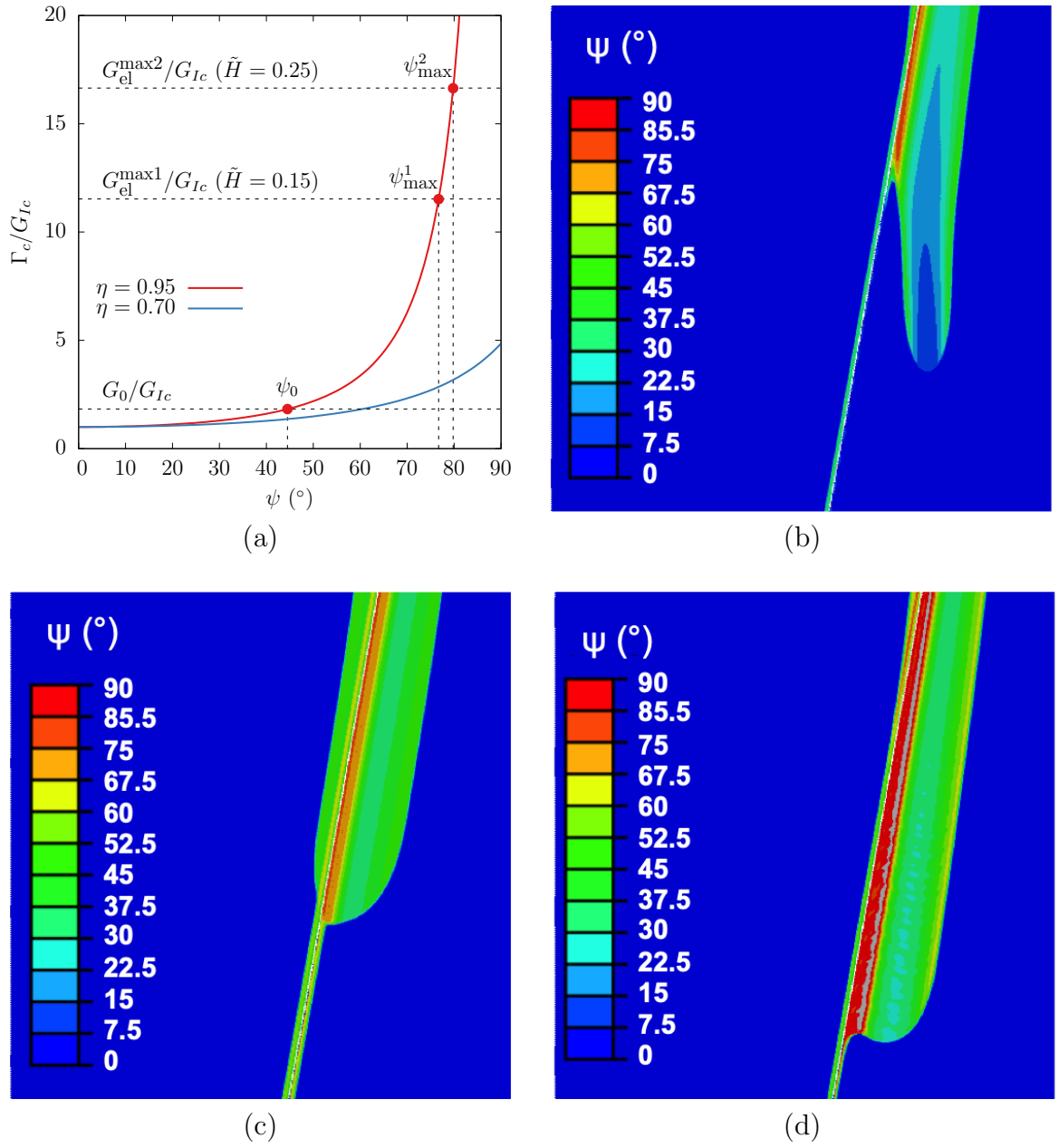

Figure 9: (a) Evolution of the dimensionless toughness Γ_c/G_{Ic} of the interface with respect to ψ for $\eta = 0.95$ and $\eta = 0.70$. Mapping of the mode mixity angle ψ (in degrees) at which the interface has been broken during the buckle propagation for two values of the step height, with $\eta = 0.95$. (b) $\tilde{H} = 0.15$. (c) $\tilde{H} = 0.25$. (d) $\tilde{H} = 0.15$ with $\eta = 0.70$.

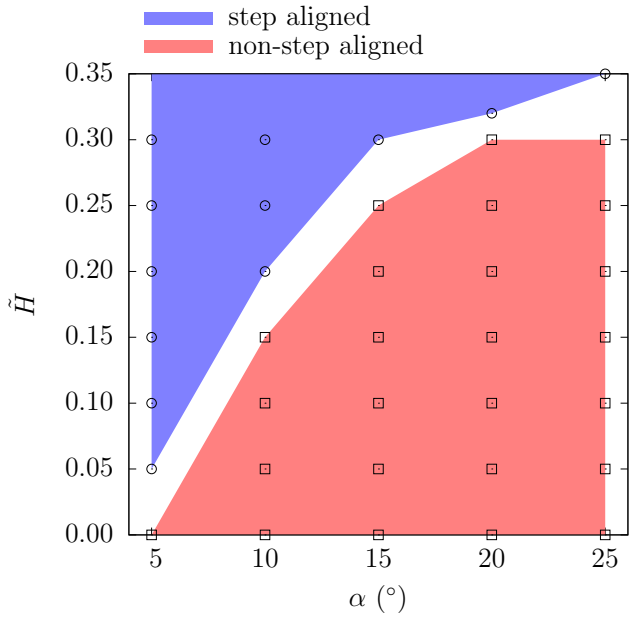

Figure 10: Propagation diagram for the buckle in the $(\alpha, \tilde{H})$ plane.

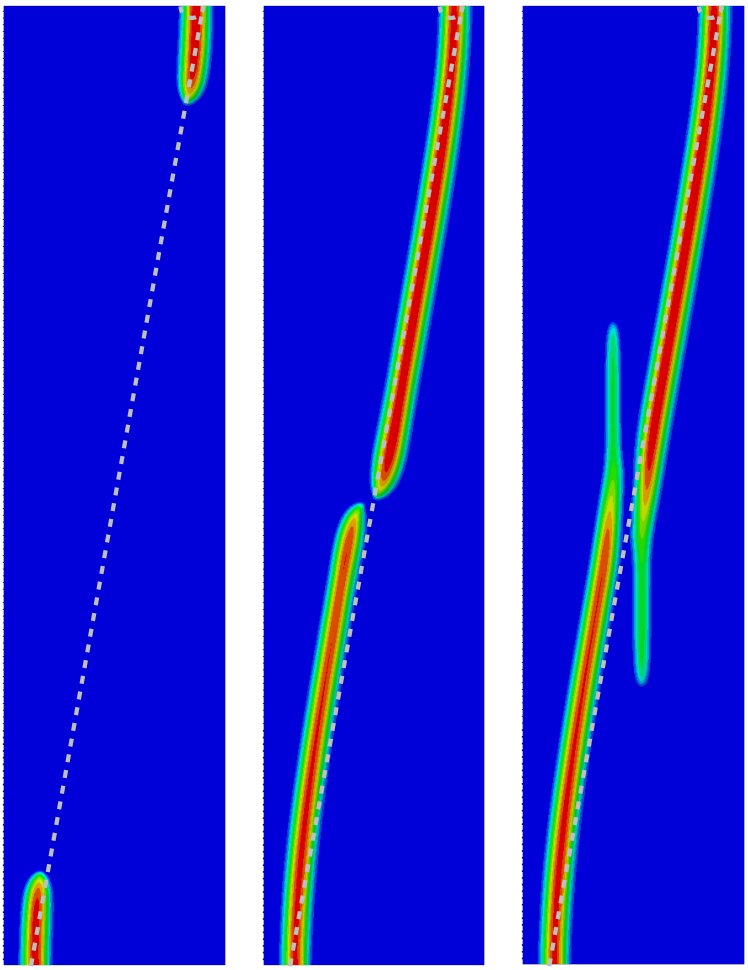

Figure 11: Propagation in two opposite directions of two buckles along a step of height $\tilde{H} = 0.3$ and tilt angle $\alpha = 10°$. The positions of the semi-circular initial defect and of the step are identified with dashed gray lines.